

Synthesis, characterization, Hirshfeld surface analysis and antioxidant activity of a novel organic-inorganic hybrid material 1-methylpiperazine-1,4-diium trioxonitrate

S. Gatfaoui, A. Mezni, T. Roisnel, H. Marouani

▶ **To cite this version:**

S. Gatfaoui, A. Mezni, T. Roisnel, H. Marouani. Synthesis, characterization, Hirshfeld surface analysis and antioxidant activity of a novel organic-inorganic hybrid material 1-methylpiperazine-1,4-diium trioxonitrate. Journal of Molecular Structure, 2017, 1139, pp.52–59. 10.1016/j.molstruc.2017.03.028 . hal-01515136

HAL Id: hal-01515136

https://univ-rennes.hal.science/hal-01515136

Submitted on 27 Apr 2017

HAL is a multi-disciplinary open access archive for the deposit and dissemination of scientific research documents, whether they are published or not. The documents may come from teaching and research institutions in France or abroad, or from public or private research centers.

L'archive ouverte pluridisciplinaire **HAL**, est destinée au dépôt et à la diffusion de documents scientifiques de niveau recherche, publiés ou non, émanant des établissements d'enseignement et de recherche français ou étrangers, des laboratoires publics ou privés.

Elsevier Editorial System(tm) for Journal of Molecular Structure

Manuscript Draft

Manuscript Number:

Title: Synthesis, characterization, Hirshfeld surface analysis and antioxidant activity of a novel organic-inorganic hybrid material 1-methylpiperazine-1,4-diium trioxonitrate

Article Type: Research Paper

Keywords: Hybrids; Crystal structure; Hirshfeld surface; Enrichment ratio; Antioxidant activity.

Corresponding Author: Dr. Houda Marouani,

Corresponding Author's Institution: Faculty of siences Bizerte

First Author: Sofian Gatfaoui

Order of Authors: Sofian Gatfaoui; Ali Mezni; Thierry roisnel; Houda Marouani

Highlights

- A new organic–inorganic hybrid trioxonitrate was synthesized at room temperature.
- The atomic arrangement shows three-dimensional network.
- The crystal packing stabilized by a set of hydrogen bonds also analyzed by Hirshfeld surface.
- This compound was investigated by IR spectroscopy.
- Antioxidant study, *in vitro*, shows significant scavenging capacity of free radicals (DPPH• and ABTS•).

*Manuscript
Click here to view linked References

Synthesis, characterization, Hirshfeld surface analysis and antioxidant activity of a novel organic-inorganic hybrid material 1-methylpiperazine-1,4-diium trioxonitrate

Sofian Gatfaoui [(a)*], Ali Mezni[(b)], Thierry Roisnel[(c)] and Houda Marouani[(a)]
(a) Laboratoire de chimie des matériaux, Faculté des Sciences de Bizerte, Université de Carthage, 7021 Zarzouna, Tunisia
(b) Département de science de la vie, Faculté des Sciences de Bizerte, Université de Carthage, 7021 Zarzouna, Tunisia
(c) Centre de Diffractométrie X, UMR 6226 CNRS, Unité Sciences Chimiques de Rennes, Université de Rennes I, 263 Avenue du Général Leclerc, 35042 Rennes, France

*Corresponding author: houdamarouani2015@gmail.com

ABSTRACT

The new inorganic-organic hybrid material 1-methylpiperazine-1,4-diium trioxonitrate (MPN) have been synthesized and crystallized to the orthorhombic system with space group Pnma and the lattice parameters obtained are a = 10.9385(9) Å, b = 6.5698 Å (4), c = 13.7021(10) Å, V = 984.68(12) $Å^3$ and Z = 4. The trigonal (NO_3^-) anions are connected to the 1-methylpiperazine-1,4-diium cations via a large number of bifurcated and non-bifurcated N-H…O and C-H…O hydrogen bonds. The diprotonated piperazine ring adopts a chair conformation, with the methyl group occupying an equatorial position. Intermolecular interactions in the crystal structure were quantified by Hirshfeld surface analysis. Infrared spectrum confirms the existence of the functional groups in the elaborated material. Optical absorption reveals an important band gap energy indicating stability of the title compound. The DTA/TGA and DSC curves indicate that the crystal is thermally stable up to 180 °C. The antioxidant properties were determined via the DPPH radical scavenging, the ABTS radical scavenging, hydroxyl radical scavenging and ferric reducing power (FRP).

KEY WORDS: Hybrids; Crystal structure; Hirshfeld surface; Enrichment ratio; Antioxidant activity.

1. Introduction

A hybrid material is qualified when it comprises both organic and inorganic entities. The synergy between the thermal, optical and / or electrical properties of inorganic particles and the physicochemical properties of organic materials opens a scope for these objects in various fields' namely optical, electrical conductivity and photochemistry [1-6]. The hybrid materials also penetrate application fields in the photo-catalysts [7, 8] as well as biology [9-11] and medicine [12-14]. The structure of hybrid materials can be divided into two classes and in that function of levels of interaction between the organic and the inorganic phase [15]. Class I materials correspond to systems in which organic and inorganic components are linked by low-energy bonds. Class II materials correspond to systems where both components are linked together by high-energy bonds. The contribution of this work is on hybrid materials based on nitrate, they are developed by grafting a nitrate anion of an organic matrix, more particularly 1-methylpiperazine. On the other hand, the piperazine and its derivatives are widely used due to their interesting biological and pharmacology proprieties [16]. In these hybrid materials the nitrate anions and organic cations are ensured by electrostatic and van der Waals interactions which, together with hydrogen bonds, build a two-dimensional [17] or three-dimensional networks [18]. We report in this work chemical preparation, crystal structure study, Hirshfeld analysis, infrared spectroscopy, Optical absorption, thermal analysis and antioxidant activity of a novel organic trioxonitrate, $C_5H_{14}N_2(NO_3)_2$.

2. Experimental

2.1. Chemical preparation

An aqueous solution containing 2 mmol of HNO_3 in 10 mL of water was added to 1 mmol of 1-methylpiperzine in 10 mL of ethanol. The obtained solution was stirred for 30 min and then left to stand at room temperature. Colorless prisms of the title compound were obtained after some days. Schematically the reaction can be written:

$C_5H_{12}N_2 + 2HNO_3 \longrightarrow C_5H_{14}N_2(NO_3)_2$

Crystallographic data (CIF) for the structure reported in this paper have been deposited in the Cambridge Crystallographic Data centre as supplementary materials N° CCDC 1479741. Copies of the data can be obtained, free of charge, from the Cambridge Crystallographic Data Centre via www.ccdc.cam.ac.uk/data_request/cif.

2.2. Investigation techniques

2.2.1. X-ray Crystallography

The intensity data were collected at 150 K using an APEXII, Bruker-AXS diffractometer with MoKα radiation (λ = 0.71073 Å). Absorption corrections were performed using the multi-scan technique using the SADABS program [19]. The total number of measured reflections was 3785 among which 1213 were independent and 961 had intensity $I > 2\sigma(I)$. The structure was solved by direct methods using the *SIR97* program [20] and then refined with full-matrix least-square methods based on F^2 (*SHELXL-97*) [21] with the aid of the *WINGX* program [22]. All non-hydrogen atoms were refined with anisotropic atomic displacement parameters. The hydrogen atoms bonded to nitrogen atoms were located from a difference map. The rest of the H atoms were treated as riding, with C—H = 0.99 Å (methylene), or 0.98 Å (methyl), with $U_{iso}(H) = 1.2U_{eq}$(C-metylene atoms) and$1.5U_{eq}$(C-methyl atoms).

A final refinement on F^2 converged at $R(F^2) = 0.044$ and $wR(F^2) = 0.108$. The parameters used for the X-ray data collection as well as the strategy for the crystal structure determination and its final results are reported in Table 1. An ORTEP [22] drawing of the molecular structure is shown in Fig. 1.

2.2.2. Physical measurements

IR spectrum was recorded in the range 4000 - 400 cm^{-1} with a with a NICOLET IR 200 FT-IR infrared spectrometer.

UV–Vis spectrum was recorded on a Perkin-Elmer Lambda 19 spectrophotometer in the 200–800 nm range.

Thermal analysis was performed using a multimodule 92 Setaram analyzer operating from room temperature up to 500 °C at an average heating rate of 10 °C/min and the mass of the simple was 15.18 mg for DTA/TGA and 10 mg for DSC.

2.3. Antioxidant activity $[C_5H_{16}N_2](NO_3)_2$ (MPN)

2.3.1. DPPH radical scavenging activity

The free-radical scavenging activity of the various concentrations of new compound (MPN), and ascorbic acid was measured with the stable radical diphenylpicrylhydrazyl (DPPH) in terms of radical-scavenging activity. 3 mL of DPPH (in methanol) was added to 100 µL of compound (dissolved in methanol), at different concentrations (1- 0.2 mg/mL). After incubation 30 min, the absorbance was measured at 517 nm according to a described procedure [23]. Ascorbic acid was used as a positive control. Each study corresponded to three experiments, performed in duplicate. The scavenging activity was estimated based on the percentage of DPPH radicals scavenged by the following formula:

DPPH radicals scavenged activity (%) = $[(A_{cont} - A_{test})/A_{cont}] \times 100$ where A_{cont} is absorbance of control, A_{test} is absorbance of tested extract solution.

2.3.2. ABTS radical scavenging activity

ABTS assay was performed according to the protocol [24]. The stock solution was prepared by mixing equal volumes of 7 mM ABTS solution and 2.45 mM potassium persulfate solution followed by incubation for 12 h at room temperature in the dark to yield a dark-colored solution containing ABTS•+ radicals. Working solution was prepared freshly

before each assay by diluting the stock solution by mixing of stock solution to 50% methanol. Free radical scavenging activity was assessed by mixing 300 μL of compound (MPN) at various concentrations (1-0.2 mg/mL in methanol) with 3.0 mL of ABTS working standard. The absorbance was measured at 734 nm. Data for each assay was recorded in triplicate. Ascorbic acid was used as positive controls. The scavenging activity was estimated based on the percentage of ABTS radicals scavenged by the following formula:

$$\text{ABTS radicals scavenged activity (\%)} = [(A_{cont} - A_{test}) / A_{cont}] \times 100$$

Where A_{cont} is absorption of control, A_{test} is absorption of tested compound.

2.3.3. Hydroxyl radical scavenging ability

The effect of compound on hydroxyl radicals was assayed by using the deoxyribose method described by Halliwell and Gutteridge [25]. 2-Deoxyribose is degraded on exposure to hydroxyl radicals generated by Fenton's reaction. The compound (MPN) and ascorbic acid (AA) was prepared in methanol. The reaction mixture contained 450 μL of 0.2 M sodium phosphate buffer (pH 7.0), 150 μL of 10 mM 2-deoxyribose, 150 μL of 10 mM $FeSO_4$-EDTA, 150 μL of 10 mM H_2O_2, 525 μL of H_2O, and 75 μL of sample solution (0.2 - 1 mg/mL). The reaction was started by the addition of H_2O_2. After incubation at 37°C for 30 min, the reaction was stopped by adding 750 μL of 2.8% trichloroacetic acid and 750 μL of 1% TBA in 50 mM NaOH, the solution was boiled for 10 min, and then cooled in water. The absorbance of the solution was measured at 520 nm. Ascorbic acid (0.2 - 1 mg/mL) was used as a positive control. The ability to scavenge the hydroxyl radical was calculated using the following equation:

$$\text{OH radical scavenging ability (\%)} = [(A_{cont} - A_{test}) / A_{cont}] \times 100$$

A_{cont} = absorbance of the control (reacting mixture without the test sample), and A_{test} = absorbance of reacting mixture with the test sample.

2.3.4. Reducing propriety

The reducing power of new compound (MPN) was assayed according to the method of Pulido et al (2000) [26]. Briefly, a methanolic solution of compound (MPN) (1 mL) at different concentration (0.2-1mg/mL) was mixed with 2.5 mL of phosphate buffer (0.2 M) and 2.5 mL of 1% potassium ferricyanide and incubated at 50 °C for 20 min. To this mixture, 2.5 mL of 10% trichloroacetic acid was added and the mixture was centrifuged at 3000 rpm for 20 min. The upper layer (2.5 mL) was mixed with 2.5 mL of deionized water and 0.5 mL of 0.1% Ferric chloride and the same treatment was performed to a standard ascorbic acid solution and the absorbance taken at 700 nm. The reducing property was measured using the following equation:

$$\text{Reducing power (\%)} = [(A_{cont} - A_{test}) / A_{cont}] \times 100$$

Where A_{cont} = absorbance of the control (reacting mixture without the test sample), and A_{test} = absorbance of reacting mixture with the test sample.

3. Results and discussion

3.1. Structure description

The asymmetric unit of the title salt, $C_5H_{14}N_2^{2+}.2NO_3^-$ contains a half of 1-methylpiperzine-1,4-diium dications and two independent nitrate anions (Fig.1). Both kinds of ions have mirror planes passing through the entire nitrate anions and the N3, H3, N4, H4A, H4B and the methyl C atom of the $C_5H_{14}N_2^{2+}$.

In the title compound, the diprotonated 1-methylpiperazine are linked to the nitrate anions by multiple bifurcated N-H…O(O,O) and weak C-H…O hydrogen bonds, forming a three-dimensional network, with donor-acceptor distances varying between 2,737(2) and 3,475(19) Å (Fig.2). Interatomic bond lengths and angles of the nitrate anions spread respectively within the ranges 1.232(2) – 1.263(2) Å and 118.62(18) – 120.80(17)°. These geometrical features have also been noticed in other related crystal structures [17, 18, 27]. It is

worth noting that N1—O1, N1—O3 and N2—O4 distances are very long that another nitrogen-oxygen atoms, because O1, O3 and O4 are applied in strong hydrogen bonds (table 3) while the remaining oxygen atoms are applied in weak hydrogen bonds. Geometrical parameters of the 1-methylpiperazin-1,4-dium dications are found to be in agreement with those of another similar structures of 1-methylpiperazin-1,4-diium dipicrate [28], 1-methylpiperazinediium tetrasulfidotungstate monohydrate [29], 1-Methylpiperazine-1,4-dium bis(hydrogen oxalate) [30] and Bis(1-methylpiperazine-1,4-diium) di-μ-bromido-bis[tetrabromidobismuthate(III)] dihydrate [31]. The cyclic diamine adopts a chair confirmation with the methyl group occupying the equatorial position proved by the torsion angles C3-N3-C1-C2 : 175.28(14)° and C3-N3-C1^{i}-C2^{i}: -175.28(14)° [i: x, -y + ½, z], with puckering parameters: Q = 1.2556 Å, θ = 90° and φ = -16 ° [32] and atoms N3 and N4 deviating by -0.341 and 0.229 Å, respectively from the least-squares plane defined by the remaining atoms in the ring.

The 1-methylpiperzine-1,4-diium are located around the mirror y = 1/4 and ¾ of the orthorhombic cell. The C-C distance is equal to 1,507(2) Å and the N–C distances, the C–N–C and C–C–N angles are similar and lie within the ranges 1,485(3) – 1.5005 (17) Å, and 108,93(15) – 112,19(16)°, respectively.

The crystal structure of $(C_5H_{14}N_2)(NO_3)_2$ is stabilized by an involved three-dimensional hydrogen bonding arrangement (Table 3). The nitrate oxygen atoms are implicated in hydrogen bonding as acceptors while the protonated amine groups are exclusively donors. Moreover, this structure exhibits two types of hydrogen bonds, the first type, N–H…O, with D…A distance ranging from 2.737(2) to 3.282(3) Å. While the second one, C–H…O, with D…A distance spreading from 3.077(2) to 3.4753(19) Å. A three-dimensional frame work is then created.

In order to quantify the various intermolecular interactions, Hirshfeld surface [33] and their associated finger print plots [34] were calculated using Crystal Explorer 3.1 [35].

3.2. Hirshfeld Surface Analysis

The 3D Hirshfeld surfaces and 2D fingerprint maps are unique for each molecule in the asymmetric unit of a given crystal. The Hirshfeld d_{norm} surfaces of 1-methylpiperazine-1,4-dium dinitrate are shown in Fig. 3. The normalized contact distance (d_{norm}) based on both d_e, d_i and the vdw radii of the atom, given by Eq. (1) enables identification of the regions of particular importance to intermolecular interactions [36]: red regions (distances shorter than sum of vdW radii), white region (represent the distance of contact which is exactly the vdW separation), blue regions (distances longer than sum of vdW radii). The red regions on the d_{norm} surface illustrate the significant N-H…O and C-H…O hydrogen bonding between ammonium group and nitrate anion.

$$\boldsymbol{d_{norm}} = \frac{\boldsymbol{d_i - r_i^{vdW}}}{\boldsymbol{r_i^{vdW}}} + \frac{\boldsymbol{d_e - r_e^{vdW}}}{\boldsymbol{r_e^{vdW}}} \quad \textbf{(1)}$$

Here, we estimate the intermolecular contacts, which are shown in Fig. 4. The above analysis (Fig. 5) can be done by quantitative calculation of 2D fingerprint polts through the CrystalExplorer program. This figure represents the major contributors contacts on the surface of Hirshfeld namely H ... H and O ... H / H ... O contacts. The interatomic contacts O…H / H…O have the greatest contribution to the surface of Hirshfeld (71.2%), they are represented by two sharp symmetric spikes in the two-dimensional fingerprint maps, with a maximum $d_e + d_i \sim 1.83$Å (Fig. 5a). This value is less than the sum of van der Waals radii of oxygen (1.52 Å) and hydrogen (1.09Å) atoms; it confirms that the inter-contact is considered as being close contact. The H…H contacts appear in the middle of the scattered points in the two-

dimensional fingerprint maps; they comprise 23% of the entire surface of Hirshfeld. The round single peak at $d_e + d_i \sim 2.3$Å (Fig. 5b) results from a long interatomic H…H contact.

The enrichment ratio (ER) of a pair of elements is defined as the ratio between the proportion of actual contacts in the crystal and the theoretical proportion of random contacts [37]. The enrichment of contacts was calculated for all the sum of single moieties present in the molecule (Table 4). The ER value of approximately 1.54 and 1.93 for the O…H/H…O and O…N/N…O contacts respectively clearly provides evidence for the formation of N-H…O interactions. The H…H contacts are the second most frequent interactions due to the large quantity of hydrogen on the molecular surface (23.2 %), but they have too small degree figured with an enrichment ratio of 0.66 [38]. The group 1-methylpiperazine-1,4-diium is devoid of double and triple bonds. This chemical edifice has a large number of hydrogen atoms on their surface (S_H = 59.1 %), on the other hand carbon atoms are rarely present at the molecular surface (S_C = 0 %), as they generally form four bonds with other atoms, therefore we can notice that the C…C contacts are completely disfavored in ($C_5H_{14}N_2^{2+}$) with an enrichment ratio (E_{cc} = 0). The ER relates to the contacts of O...O and N...H/H...N are of low meaning as they are derived from less important interactions with small contributions in the all parts Hirshfeld surface.

The electrostatic potentials were determined by TONTO [39] integrated with Crystal explorer 3.1 [35] and were represented on Hirshfeld surfaces employing the STO-3G basis level over a range ±0.14 a.u. The presence of N-H…O interactions between the pair of (NO_3^-) anions and ($C_5H_{14}N_2^{2+}$) cations can be observed trough their corresponding Hirshfeld surfaces mapped over the electrostatic potential (**Fig. 6**). In addition, the negative potential around the oxygen atoms (acceptors) appear as light-red cloud and the positive potential (donors) around 1-methylpiperazine-1,4-diium nitrogen atoms as a light-blue cloud.

Such visual analysis for intermolecular interactions is coherent with those noticed by the X-ray diffraction analysis.

3.3. Vibrational studies of $C_5H_{14}N_2(NO_3)_2$

To gain information on the crystal structure, we have undertaken a vibrational study using infrared absorption. The infrared spectrum of MPN measured between 4000 and 400 cm^{-1} and recorded at room temperature is shown in Fig. 7. Although a detailed assignment of all the bands is difficult, the most important attribution mode is realized by comparison with similar compounds and to the literature [40-42]. NO_3^- is planar and has three equivalent N–O bonds (D_{3h} symmetry). The six vibrational (3N-6) degrees of freedom lead to two bending and two stretching modes, of which two are doubly degenerate. The two bending modes (E′ and $A_2^{''}$) are infrared-active but have low intensity. The symmetric stretching vibration ν1 ($A_1^{'}$) is not infrared-active, while the degenerate ν3 (E') asymmetric stretching vibration is infrared-active. The results of the infrared spectroscopic analyze are reported in Table 1. Two sharp bands are observed at 1176 and 1093 cm^{-1}. The bands are assigned to the ν_1 NO_3 symmetric stretching vibration. Two intense bands are observed at 1397 and 1314 cm^{-1} and may be assigned to the ν_3 NO_3 asymmetric stretching vibration. The bands between 900 and 688 cm^{-1} are assigned to the ν_3 NON in-plan bending mode. The bands at 1028 and 992 cm^{-1} attributed to the out-of-plan bending vibrations ν_2.

In the high-frequency region between 3090 and 2590 cm^{-1}, the observed bands correspond to the stretching vibrations of the NH, NH_2, CH_2 and CH_3 groups. Weak N–H···O bonds (2,737(2) – 3,282(3) Å) are manifested in the vibrational spectrum as perturbed NH^+ and NH_2^+ groups vibrations of the diprotonated piperazinium cations. The most intense IR band in experimental spectrum, located at 1663 cm^{-1}, corresponds to the deformation mode δ(NH). The deformation modes of the double bonds –CH_2 and -CH_3 and the stretching mode

of the bond C-N are assigned to bands located between 1550 and 1300 cm^{-1}. The bands with frequency at 1176, 1084, 1047 and 909 cm^{-1} are ascribed for the δ(C-N), ν(C-C), δ(C-H) and δ(N-H). Finally, those bands seen at 826, 756, 752 and 688 are credited to CCN and CNC deformation respectively.

3.4. UV absorption of $C_5H_{14}N_2(NO_3)_2$

The UV–Visible spectra of 1-methylpiperazine-1,4-dium dinitrate in ethanol solution shows one broad band at λ = 302 nm (Fig. 8a), indicates the n→π∗ transition of the nitrate group. In addition, the electronic spectrum of $C_5H_{14}N_2(NO_3)_2$ provided by using the Tauc model [43], optical band gap of 3.8 eV as reported in Fig. 8b, suggesting that the materials may possess semiconducting properties [44].

3.5. Thermal behavior

Thermal analysis DTA-TGA of $C_5H_{14}N_2(NO_3)_2$ (Fig. 9) was performed in air with a heating rate equal to 10 °C.min^{-1}. The TGA curve shows that the title compound is stable until 180°C and the DTA curve highlights the presence of an endothermic peak at 189 °C without loss of mass. This peak corresponds to the melting of our product. Indeed treatment of our sample on a Kofler bench in the vicinity of 190 °C shows the fusion of the compound. A second peak located at 223 °C accompanied by a weight loss, this peak is assigned to the total combustion of our compound. This mass loss is related to the degradation of the organic part which is confirmed by obtaining a black residue carbon at the end of the experiment.

The analysis differential scanning calorimetry of $C_5H_{14}N_2(NO_3)_2$ conducted under atmosphere of argon and with a heating rate equal 5 K.min^{-1}. The DSC diagram shown in Fig. 10 highlights an endothermic peak around 187 °C ($\Delta H_{melting}$ = 26.24 kJ.mol^{-1}) followed by an exothermic combustion at 212 °C. These two phenomena are also previously observed by differential thermal analysis (DTA).

3.6. In vitro antioxidant activity $[C_5H_{16}N_2](NO_3)_2$ (MPN)

The most abundant free radicals in biological systems are the oxygen-centered free radicals and their metabolites, usually referred to as ROS [45]. ROS are formed continuously as normal by-products of cellular metabolism; and, in low concentrations, they are essential for several physiological processes. However, when produced in excess, ROS can damage cell functionality as they can harm cellular lipids, proteins, and DNA [46]. Now days, interest is focused on the synthesis of new compounds with potential applications, such as cancer diagnosis and treatment of tumor [47].

The objective of this study was to evaluate the antioxidant activity of new derives compounds of MPN. The antioxidant properties were determined via the DPPH radical scavenging, the ABTS radical scavenging, ferric reducing power (FRP), hydroxyl radical scavenging and ferrous ion chelating activity (FIC).

3.6.1. DPPH radical scavenging activity

The result showed remarkable scavenging activity was presented in Fig. 11. The derive had the highest capacity of scavenging DPPH radicals with percentage of inhibition 58.69 ±0.91% (IC50=0.96 mg/mL) at the concentration (1mg/mL) and compared with ascorbic acid at the same concentration 91.35±1.048 % (IC50=0.476 mg/mL).

3.6.2. ABTS radical scavenging activity

Differences for the ABTS•+ (2, 2 azobis-(3-ethylbenzothiozoline-6-sulphonic acid) radical scavenging capacities of each sample was recorded in figure 12. The compound (MPN) was presented the highest capacity of scavenging at the high concentration (1mg/mL)

with value 40.141± 1.21% (IC50=1.115) and ascorbic acid at the same concentration 66.79±3.91 % (IC50=0.733).

3.6.3. Hydroxyl radical scavenging ability

The results were summarized in the figure 13 reported that MPN has a slight hydroxyl radical scavenging activity followed at highest concentration (1mg/mL) 38.79± 1.15 %(IC50=1.157) and compared with ascorbic acid at the same concentration (1mg/mL) the percentage of inhibition was 72.7 ± 1.86% (IC50=0.68).

3.6.4. Reducing propriety

The results was presented in figure 14 demonstrated that the most effective for reducing property to compare to that of ascorbic acid and the percentage in the highest concentration (1mg/mL) is AA 78.77± 0.94 % (IC50=0.545) and MPN 55.35±0.75 % (IC50=0.81);

4. Concluding remarks

Single crystals of $C_5H_{14}N_2(NO_3)_2$ have been productively grown at room temperature. The new compound was investigated by single crystal X-ray diffraction. Crystal structure of this compound was found to be built by trioxonitrate anions and 1-methylpiperazine-1,4-diium cations associated through manifold H-bonds type N–H…O and C-H…O, forming a three-dimensional arrangement. The Hirshfeld surface analysis reveals the percentage of intermolecular contacts of the title compound. The vibrational properties of this structure were studied by infrared spectroscopy. The assignment of the vibrational bands was performed by comparison with the vibration modes frequencies of homologous compounds. The thermal analyses illustrate the stability of MNP up to 180°C. Also the optical absorption shows the important band gap energy indicative of stability of the title compound. Furthermore this compound was found to be the applicant exhibiting antioxidant property; this is demonstrated

by scavenging DPPH radicals, ABTS radicals, reducing property and slight hydroxyl radical scavenging to that of ascorbic acid.

Acknowledgements

This work was supported by the Ministry of Higher Education and Scientific Research of Tunisia.

References

[1] P. Englebienne, A. Van. Hoonacker, Gold–conductive polymer nanoparticles: A hybrid material with enhanced photonic reactivity to environmental stimuli, J. Colloid Interface Sci. 292 (2) (2005) 445-454.

[2] Z. Heng, G. R. Newkome, C. L. Hill, Poly(polyoxometalate) Dendrimers: Molecular Prototypes of New Catalytic Materials, Angew. Chem. Int. Ed. Engl, 39 (2000) 1771.

[3] A. Müller, H. Reuter, S. Dillinger, Supramolecular Inorganic Chemistry: Small Guests in Small and Large Hosts, Angew. Chem. Int. Ed. Engl, 34 (1995) 2328.

[4] D. Hagrman, R.C. Haushalter, J. Zubieta, Three-Dimensional Organic/Inorganic Hybrid Materials Constructed from One-Dimensional Copper Diamine Coordination Polymers Linked by Bridging Oxoanion Tetrahedra: [Cu(dpe)(MoO_4)] and [Cu(dpe)(SO_4)(H_2O)] (dpe = 1,2-*trans*-(4-pyridyl)ethene), Chem. Mater. 10 (1998) 361-365.

[5] X. L. Wang, C. Qin, E.B. Wang, Y. G. Li, C. W. Hu, L. Xu, Interlocked and Interdigitated Architectures from Self-Assembly of Long Flexible Ligands and Cadmium Salts, Angew. Chem. Int. Ed. Engl, 43 (2004) 5036.

[6] C. M. Liu, D. Q. Zhang, M. Xiong, D. B. Zhu, A novel two-dimensional mixed molybdenum–vanadium polyoxometalate with two types of cobalt(II) complex fragments as bridges, Chem. Commun. 13 (2002) 1416-1417.

[7] Y. Li, Y. Yu, L. Wu, J. Zhi, Processable polyaniline/titania nanocomposites with good photocatalytic and conductivity properties prepared via peroxo-titanium complex catalyzed emulsion polymerization approach, Appl. Surf. Sci. 273 (2013) 135-143.

[8] F. Wang, S. Min, Y. Han, L. Feng, Visible-light-induced photocatalytic degradation of methylene blue with polyaniline-sensitized TiO_2 composite photocatalysts, Superlattices Microstruct. 48 (2010) 170-180.

[9] L. M. Novena, S. S. Kumar, S. Athimoolam, Improved solubility and bioactivity of theophylline (a bronchodilator drug) through its new nitrate salt analysed by experimental and theoretical approaches, J. Mol. Struct. 1116 (2016) 45-55.

[10] A. Müller, F. Peters, M. T. Pope, D. Gatteschi, Polyoxometalates: Very Large Clusters-Nanoscale Magnets, Chem. Rev. 98 (1998) 239.

[11] C. Y. Sun, S. X. Liu, D. D. Liang, K. Z. Shao, Y. H. Ren, Z. M. Su, Highly stable crystalline catalysts based on a microporous metal-organic framework and polyoxometalates, J. Am. Chem. Soc. 131 (2009) 1883-1888.

[12] A. K. Cheetham, G. Férey, T. Loiseau, Open Framework inorganic materials, Angew. Chem. Intl. Ed. 38 (1999) 3268-3292.

[13] P.V. Braun, P. Osenar, V. Tohver, S. B. Kennedy, S. I. Stupp, Nanostructure templating in inorganic solids with organic lyotropic liquid crystals, J. Am. Chem. Soc. 121 (1999) 7302-7309.

[14] M. C. Daniel, D. Astruc, Chem. Rev., Gold nanoparticles: assembly, supramolecular chemistry, quantum-size-related properties, and applications toward biology, catalysis, and nanotechnology, 104 (2004) 293-346.

[15] H. Schmidt, J. Non-Cryst. Solids, New type of non-crystalline solids between inorganic and organic materials, 73 (1985) 681-691

[16] D. J. Conrado, H. Verli, G. Neves, C. A. Fraga, E. J. Barreiro, S. M. Rates, T. Dalla-Costa, Pharmacokinetic evaluation of LASSBio-579: an N-phenylpiperazine antipsychotic prototype, J. Pharm. Pharmacol, 60 (2008) 699–707.

[17] S. Gatfaoui, H. Marouani, M. Rzaigui, 4-Methylbenzylammonium nitrate, Acta Cryst. E69 (2013) o1453.

[18] S. Gatfaoui, H. Marouani, T. Roisnel, H. Dhaouadi, Dopaminium nitrate, Acta Cryst, E70 (2014) o571–o572.

[19] Bruker (2006). APEX2, SAINT and SADABS. Bruker AXS Inc., Madison, Wisconsin, USA.

[20] A. Altomare, M. C. Burla, M. Camalli, G. L. Cascarano, C. Giacovazzo, A. Guagliardi , A. G. G. Moliterni, G. Polidori, R. Spagna, J. Appl. Cryst. 32 (1999) 115

[21] G. M. Sheldrick, Crystal structure refinement with *SHELXL*, Acta Cryst. C71 (2015) 3-8.

[22] L. J. Farrugia, *WinGX* and *ORTEP for Windows*: an update, J. Appl. Cryst. 45 (2012) 849-854.

[23] A. Brace, N. D. Tommasi, L. D. Bari, C. Pizza, M. Politi, I. Morelli, Antioxidant principles from Bauhinia terapotensis. J. Nat. Prod. 64 (2001) 892-895.

[24] R. Re, N. Pellegrini, A. Proteggente, A. Pannala, M. Yong, C. Rice-Evans, Antioxidant activity applying an improved ABTS radical cation decolorization assay, Free Rad. Biol. Med. 26 (1999) 1231-1237.

[25] B. Halliwell, J. M. C. Gutteridge, O. I. Aruoma, The deoxyribose method: a simple test tube assay for determination of rate constants for reactions of hydroxyl radicals, Anal. Biochem. 165 (1987) 215-219.

[26] R. Pulido, L. Bravo, F. Saura-Calixto, Antioxidant activity of dietary polyphenols as determined by a modified ferric reducing/antioxidant power assay, J. Agric. Food Chem. 48 (2000) 3396–3402.

[27] S. Gatfaoui, T. Roisnel, H. Dhaouadi, H. Marouani, *trans*-2,5-Dimethylpiperazine-1,4-diium dinitrate, Acta Cryst. E70 (2014) o725.

[28] G. Dutkiewicz, S. Samshuddin, B. Narayana, H. S. Yathirajan, M. Kubicki, 1-Methylpiperazine-1,4-diium dipicrate, Acta Cryst. E67 (2011) o390–o391.

[29] B. R. Srinivasan, A. R. Naik, C. Näther, W. Bensch, Synthesis and structural characterization of 1-methylpiperazinediium tetrasulfidotungstate monohydrate, Indian Journal of Chemistry 49A (2010) 437-441.

[30] M. Essid, H. Marouani, M. Rzaigui, 1-Methylpiperazine-1,4-dium bis(hydrogen oxalate), Acta Cryst. E70 (2014) o326-o327.

[31] M. Essid, T. Roisnel, H. Marouani, Bis(1-methylpiperazine-1,4-diium) di-μ-bromido-bis[tetrabromidobismuthate(III)] dehydrate, Acta Cryst. E70 (2014) m202–m203.

[32] D. Cremer, J. A. Pople, A General Definition of Ring Puckering Coordinates, J. Am. Chem. Soc. 97 (1975) 1354–1358.

[33] J. J. McKinnon, A. S. Mitchell, M. A. Spackman, Hirshfeld Surfaces: A New Tool for Visualising and Exploring Molecular Crystals, Chem. A Eur. 4 (1998) 2136.

[34] M. A. Spackman, J. J. McKinnon, Fingerprinting intermolecular interactions in molecular crystals, CrystEngComm, 4, (2002), 378.

[35] S. K. Wolff, D. J. Grimwood, J. J. McKinnon, D. Jayatilaka, M. A. Spackamn, "Crystal Explorer 3.1," University of Westren Australia, Perth, 2013.

[36] J. J. McKinnon, F. P. A. Fabbiani, M. A. Spackman, Comparison of Polymorphic Molecular Crystal Structures through Hirshfeld Surface Analysis, Cryst. Growth Des. 7 (2007)755–769.

[37] C. Jelsch, K. Ejsmont, L. Huder, The enrichment ratio of atomic contacts in crystals, an indicator derived from the Hirshfeld surface analysis, IUCrJ, 1, (2014), 119–128.

[38] C. F. Matta, J. Hernández-Trujillo, T.-H. Tang, R.F.W. Bader, Hydrogen - Hydrogen Bonding: A Stabilizing Interaction in Molecules and Crystals, Chem. Eur. J. 9 (2003), 1940-1951.

[39] D. Jayatilaka, D. J. Grimwood, A. Lee, A. Lemay, A. J. Russel, C. Taylo, S. K. Wolff, Cassam-Chenai , A. Whitton, "TONTO—A System for Computational Chemistry," 2005.

[40] M. Essid, M. Rzaigui, H. Marouani, Synthesis, characterization and antioxidant activity of a novel organic–inorganic hybrid material *trans*-2,5-dimethylpiperazine-1,4-diium pentachlorobismuthate(III) $[C_6H_{16}N_2]BiCl_5$, J. of Mol. Struct. 1117 (2016) 257-264.

[41] R. M. Silverstein, G. Clayton Besslor, T. C. Morril (1981). Spectrometric Identification of Organic Compounds, fourth ed., John Wiley, New York.

[42] A. A. El-Emam, A. S. Al-Tamimi, K. A. Al-Rashood, H. N. Misra, V. Narayan, O. Prasad, L. Sinha, Structural and spectroscopic characterization of a novel potential chemotherapeutic agent 3-(1-adamantyl)-1-{[4-(2-methoxyphenyl)piperazin- 1-yl]methyl}-4-methyl-1H-1,2,4-triazole-5(4H)-thione by first principle calculations J. Mol. Struct. 49,(2012) 1022.

[43] J. Tauc, Optical properties and electronic structure of amorphous Ge and Si, Mater. Res. Bul. 3 (1968) 37-46.

[44] W. Q. Kan, J. Yang, Y. Y. Liu, J. F. Ma, W. Q. Kan, J. Yang, Y. Y. Liu, J. F. Ma,

A series of coordination polymers based on a multidentate N-donor ligand and different polycarboxylate anions: syntheses, structures and photoluminescent properties, CrystEngComm. 14 (2012) 6271-6281.

[45] P. Rajendran, N. Nandakumar, T. Rengarajan, R. Palaniswami, E. N. Gnanadhas, U. Lakshminarasaiah, J. Gopas, I. Nishigaki, Antioxidants and human diseases. Clinica Chimica Acta 436 (2014) 332–347.

[46] N. Sugino, Roles of reactive oxygen species in the corpus luteum. Anim. Sci. J. 77 (2006) 556–65.

[47] B. Vivekanand, K. Mahendra Raj, B. H. M. Mruthyunjayaswamy, Synthesis, characterization, antimicrobial, DNA-cleavage and antioxidant activities of 3-((5-chloro-2 phenyl-1H-indol-3-ylimino) methyl)quinoline-2(1H)-thione and its metal complexes, J. of Mol. Struct. 1079 (2015) 214–224.

Figures captions

Fig. 1. *ORTEP* drawing of **$C_5H_{14}N_2(NO_3)_2$** with the atom-labeling scheme. Displacement ellipsoids are drawn at the 30 % probability level. H atoms are represented as small spheres of arbitrary radii and the hydrogen atoms of the methyl group possess occupations 0.5. Symmetry code: (i) x, -y +1/2, z

Fig. 2. Projection of **$C_5H_{14}N_2(NO_3)_2$** structure along the *c* axis.

Fig. 3. d_{norm} mapped on the Hirshfeld surface for visualizing the intermolecular interactions of the title 1-methylpiperazine-1,4-dium dinitrate compound. Color between -0.677 a.u. (blue) to 1.253 a.u. (red). Dotted lines (red) represent hydrogen bonds.

Fig. 4. Percentage of various intermolecular contacts contributed to the Hirshfeld surface.

Fig. 5. Fingerprint plots of the contacts: O…H/H…O **(a)** and H…H **(b)**. Surfaces to the right highlight the relevant surface patches associated with the specific contacts, with d_{norm} mapped in the same manner as **Fig. 1.**

Fig. 6. Electrostatic potential mapped on the Hirshfeld surface within ±0.14 a.u. blue region corresponds to the positive electrostatic potential and red region to negative electrostatic potential.

Fig. 7. Infrared absorption spectrum of **$C_5H_{14}N_2(NO_3)_2$.**

Fig. 8. Solution state UV/vis spectra of $C_5H_{14}N_2(NO_3)_2$ **(a)** and determination of the energy gap **(b)** for 1-methylpiperazine-1,4-dium dinitrate compound according to the Tauc model.

Fig. 9. DTA and TGA curves of $C_5H_{14}N_2(NO_3)_2$ at rising temperature.

Fig. 10. DSC curve of $C_5H_{14}N_2(NO_3)_2$.

Fig. 11. DPPH Radical Scavenging Activity: tested compound (MPN), AA (ascorbic acid).

Fig. 12. ABTS radical scavenging ability: tested compound (MPN), AA (ascorbic acid).

Fig. 13. OH radical scavenging ability: tested compound (MPN), AA (ascorbic acid).

Fig. 14. Reducing power assay: tested compound (MPN), AA (ascorbic acid).

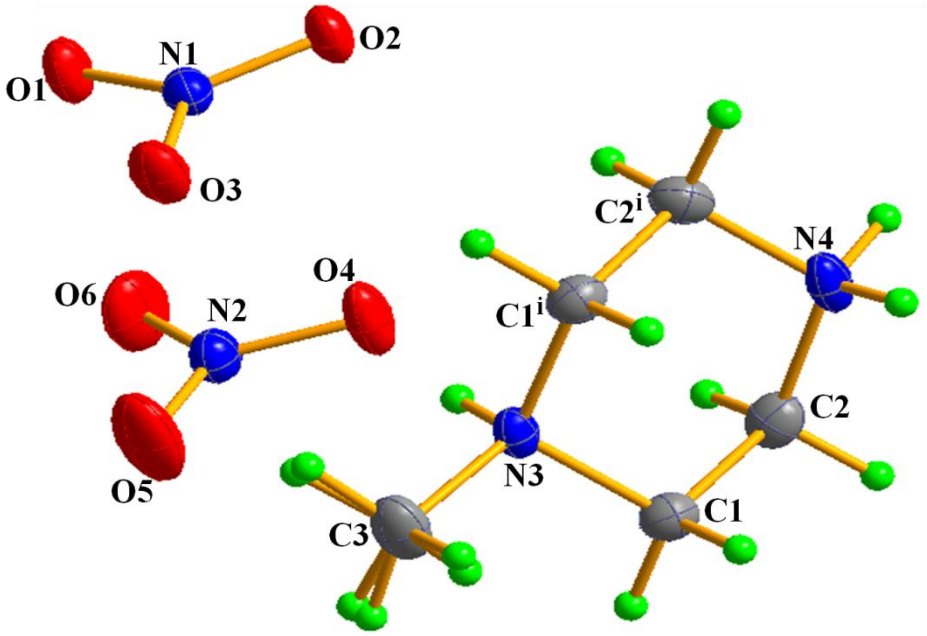


Fig. 1

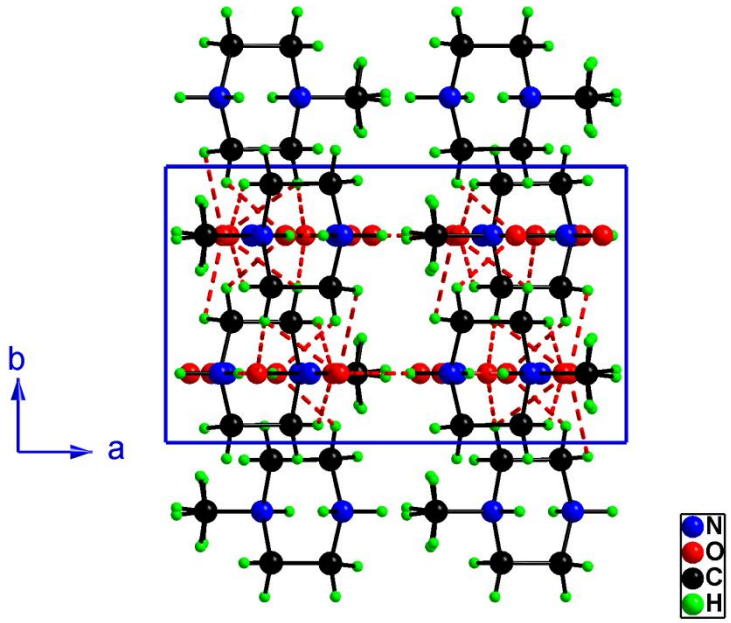


Fig. 2

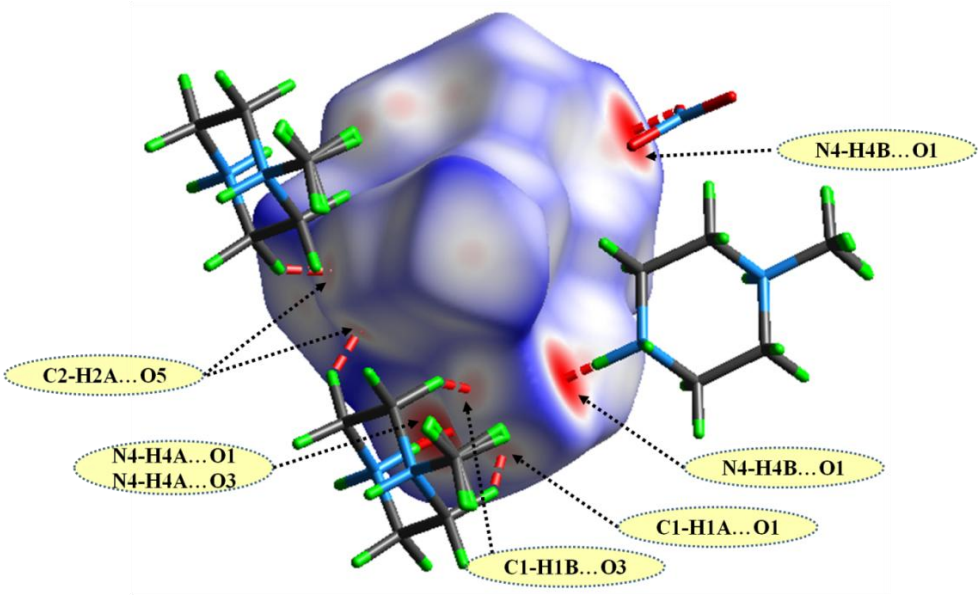


Fig. 3

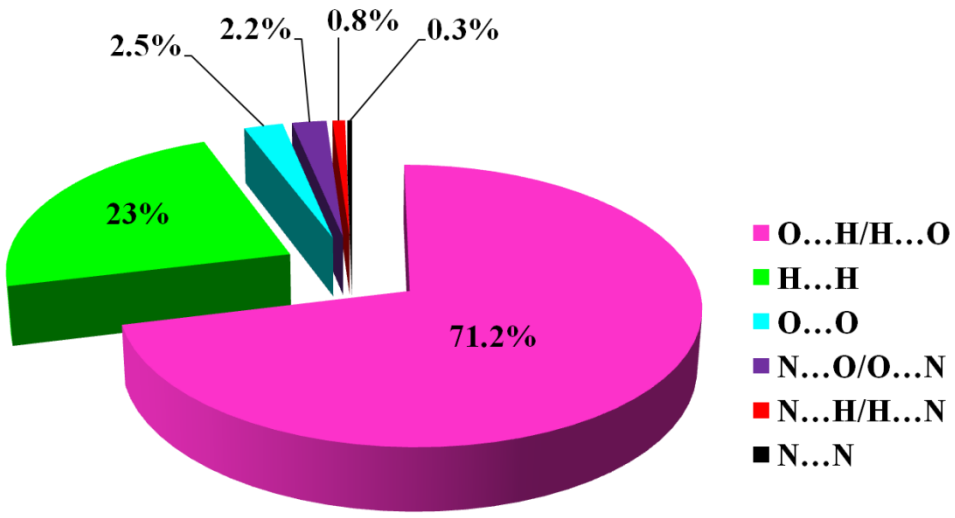


Fig. 4

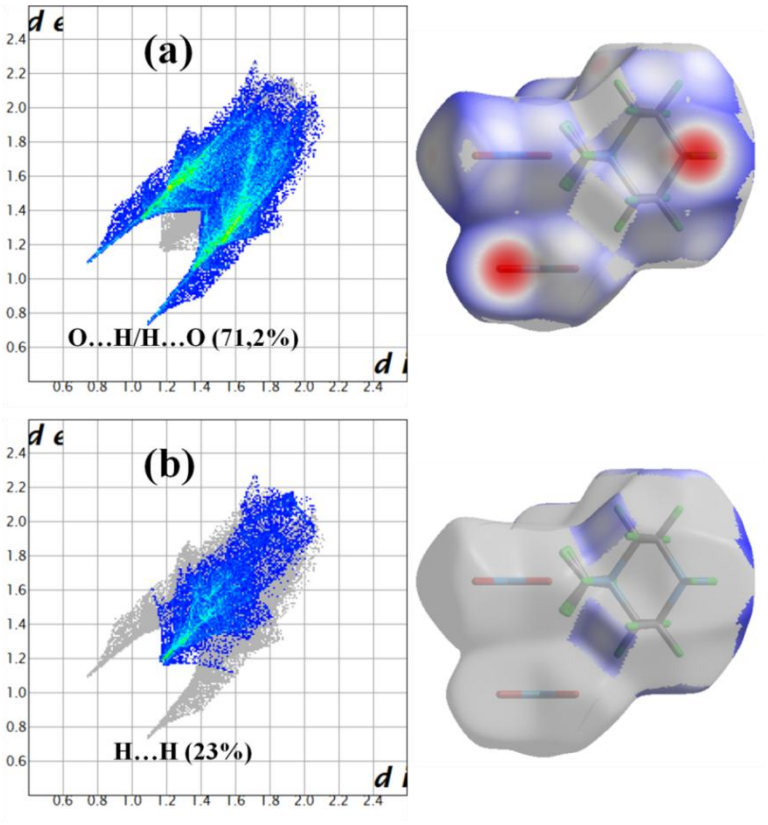


Fig. 5

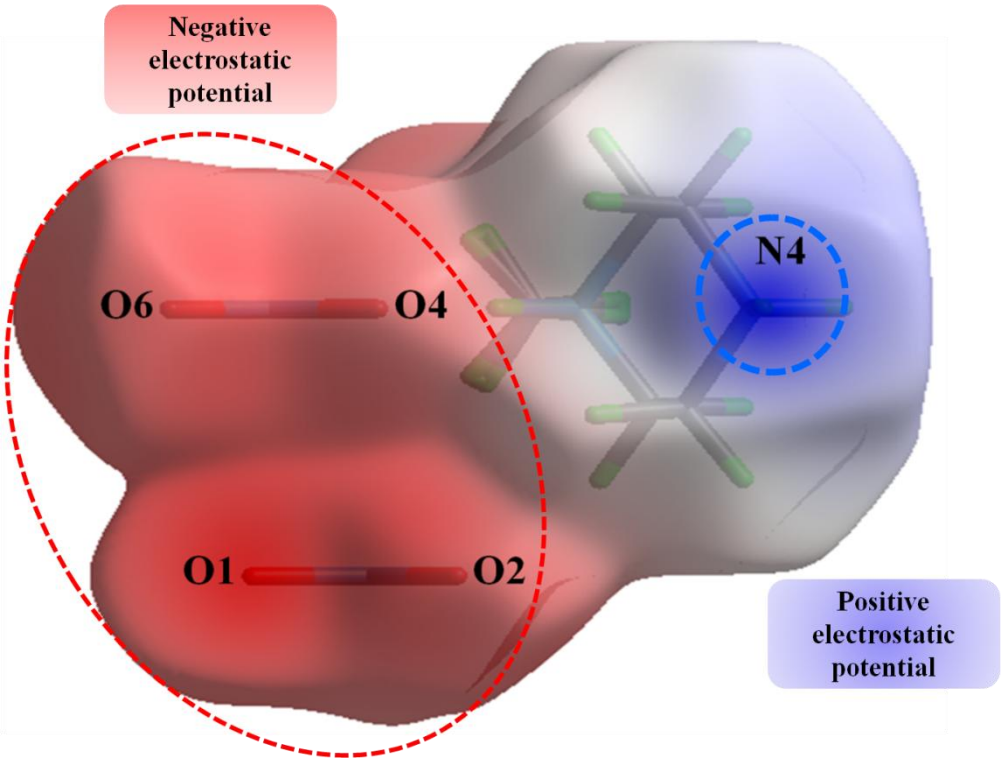

Negative electrostatic potential
O6
O4
N4
O1
O2
Positive electrostatic potential

Fig. 6

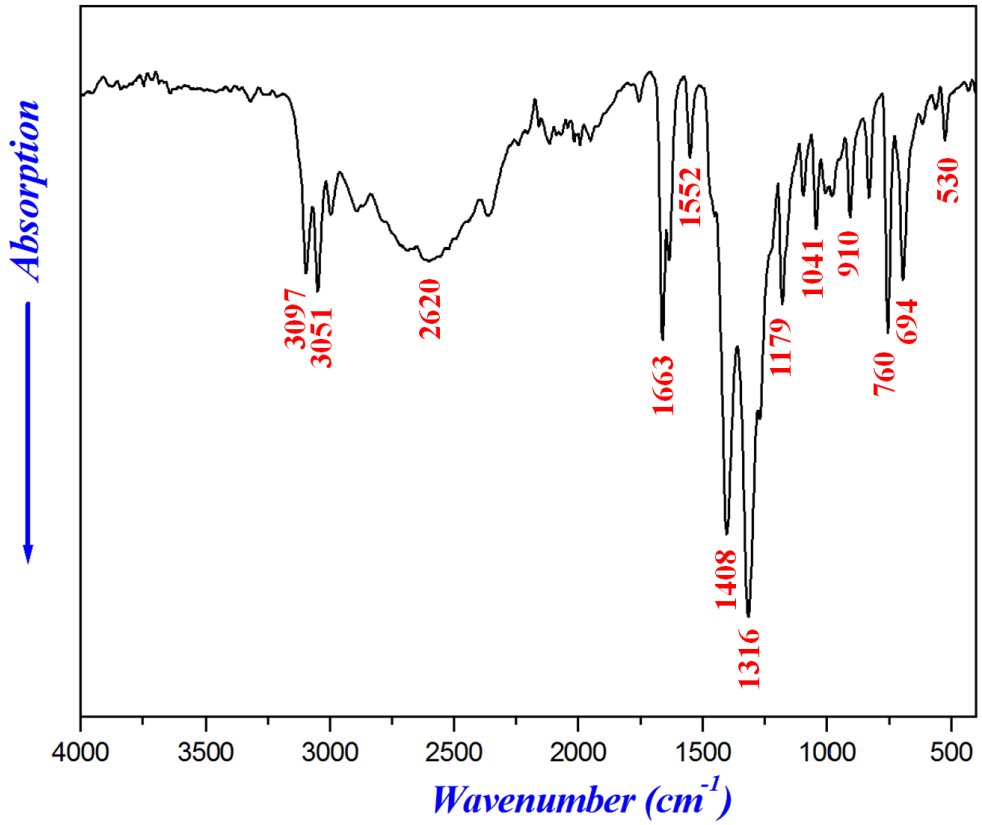

Absorption
3097
3051
2620
1663
1552
1408
1316
1179
1041
910
760
694
530
4000
3500
3000
2500
2000
1500
1000
500
Wavenumber (cm-1)

Fig. 7

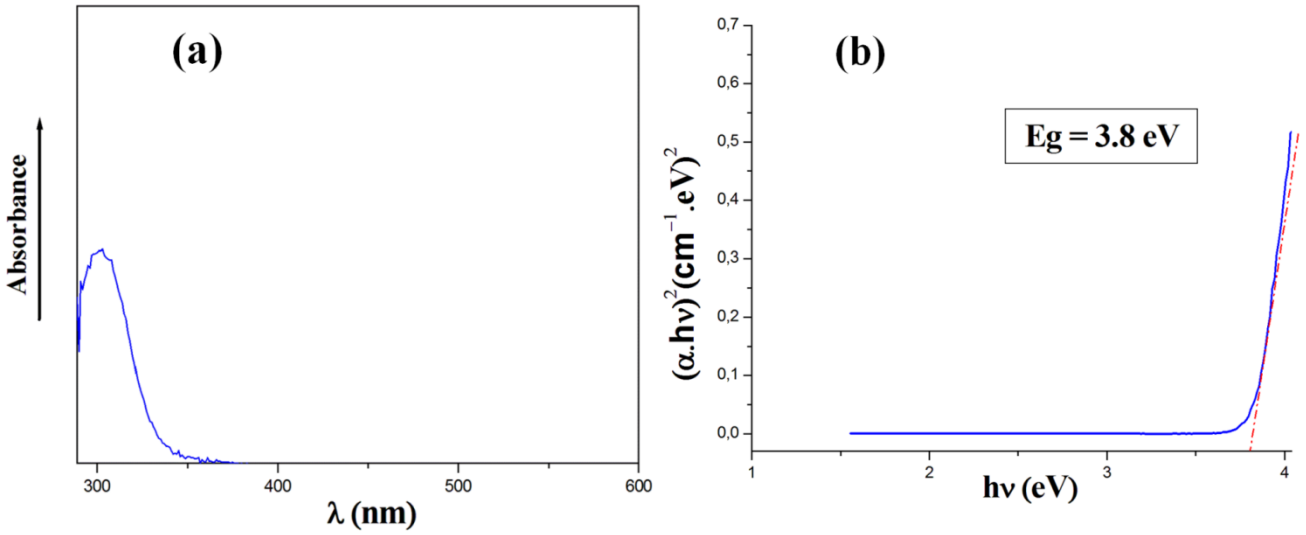

(a)
Absorbance
300
400
500
600
λ (nm)
(b)
Eg = 3.8 eV
0,7
0,6
0,5
0,4
0,3
0,2
0,1
0,0
(α.hν)²(cm⁻¹.eV)²
1
2
3
4
hν (eV)

Fig. 8

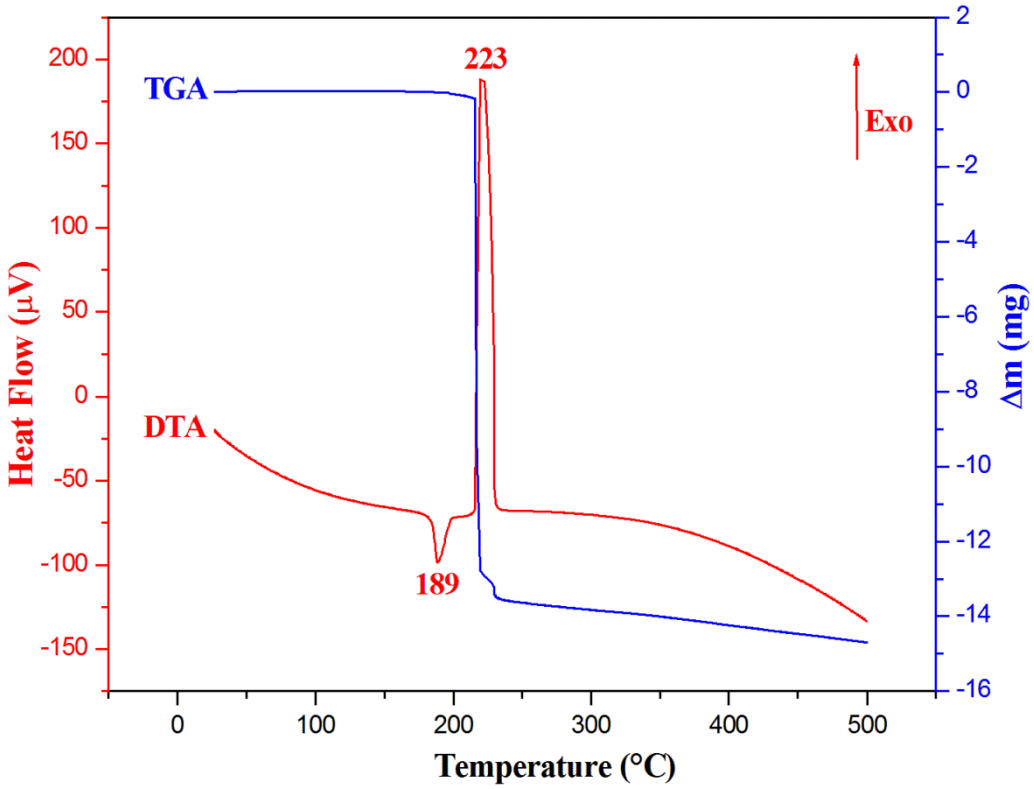

TGA
DTA
223
189
Exo
Heat Flow (μV)
Δm (mg)
Temperature (°C)
200
150
100
50
0
-50
-100
-150
2
0
-2
-4
-6
-8
-10
-12
-14
-16
0
100
200
300
400
500

Fig. 9

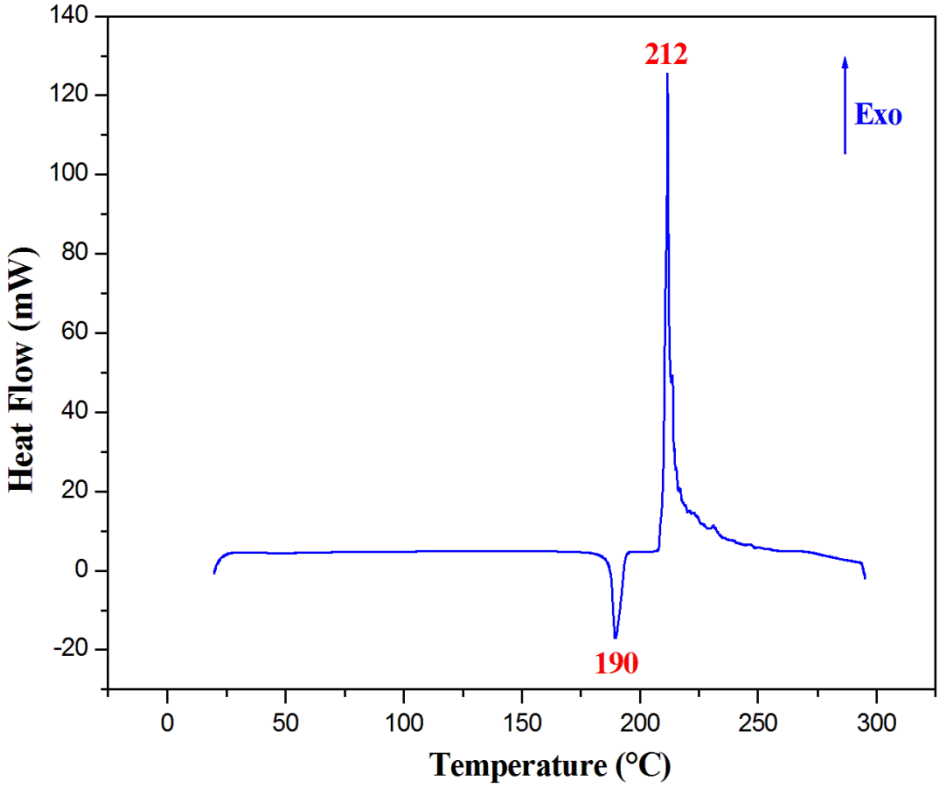

140
120
100
80
60
40
20
0
-20
Heat Flow (mW)
0
50
100
150
200
250
300
Temperature (°C)
212
190
Exo

Fig. 10

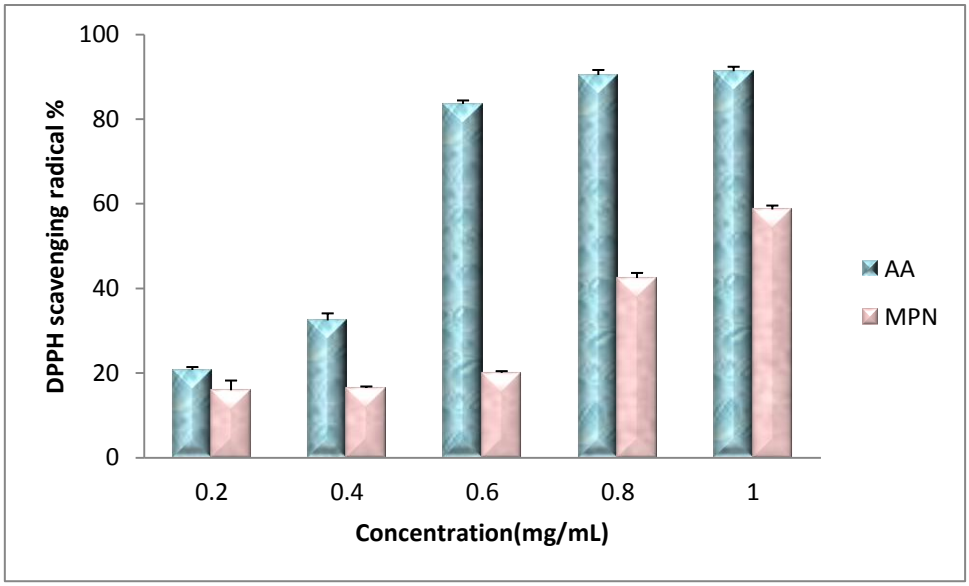

100
80
60
40
20
0
DPPH scavenging radical %
0.2
0.4
0.6
0.8
1
Concentration(mg/mL)
AA
MPN

Fig. 11

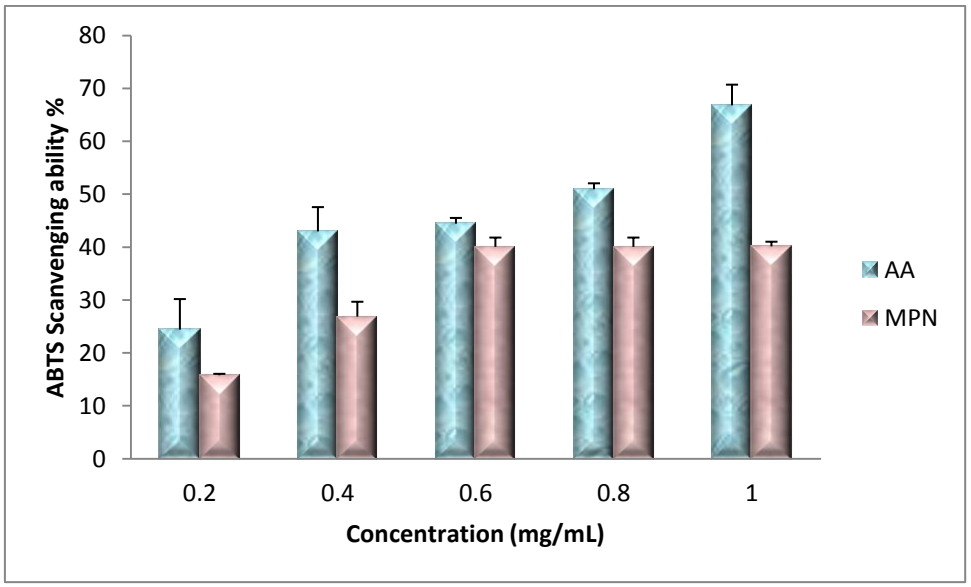

80
70
60
50
40
30
20
10
0
ABTS Scanvenging ability %
0.2
0.4
0.6
0.8
1
Concentration (mg/mL)
AA
MPN

Fig. 12

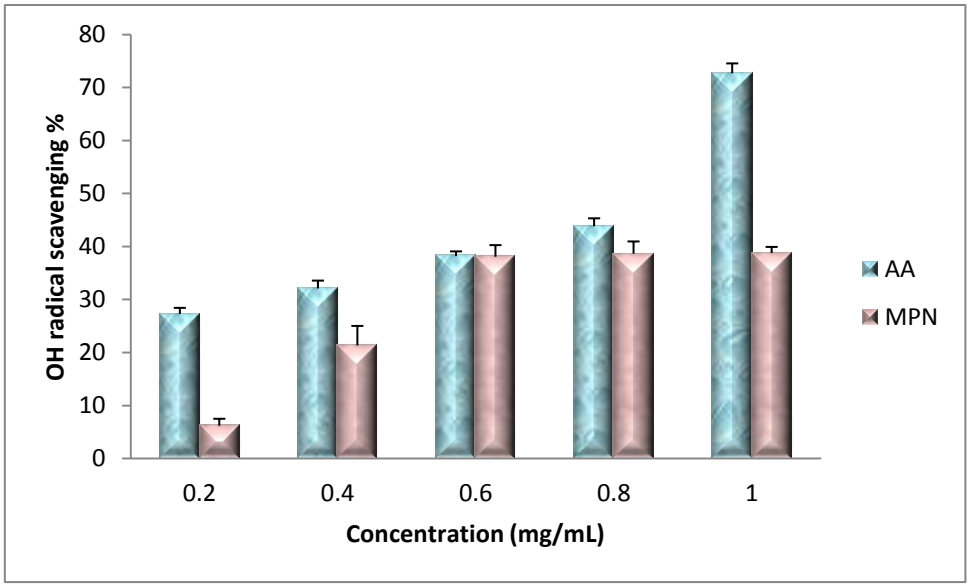

80
70
60
50
40
30
20
10
0
OH radical scavenging %
0.2
0.4
0.6
0.8
1
Concentration (mg/mL)
AA
MPN

Fig. 13

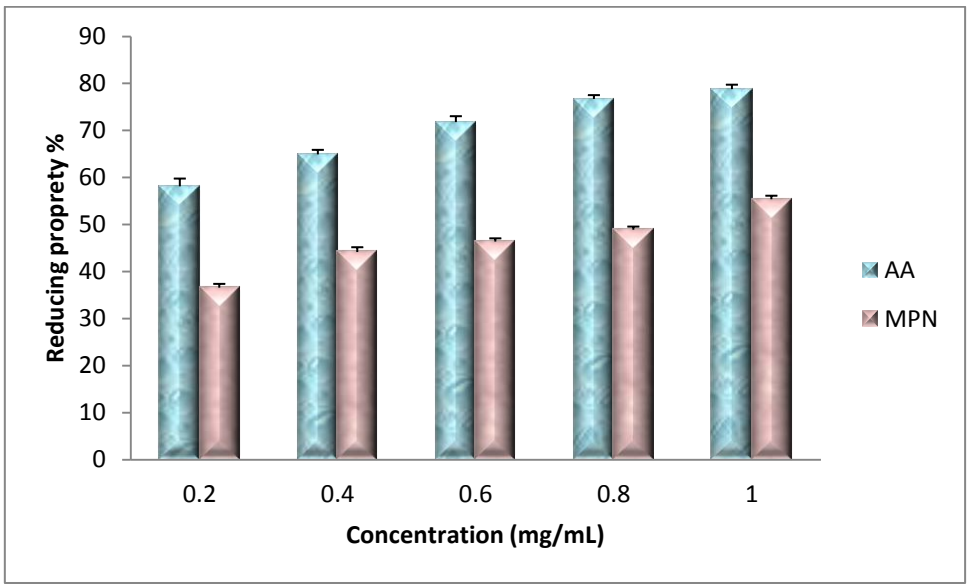
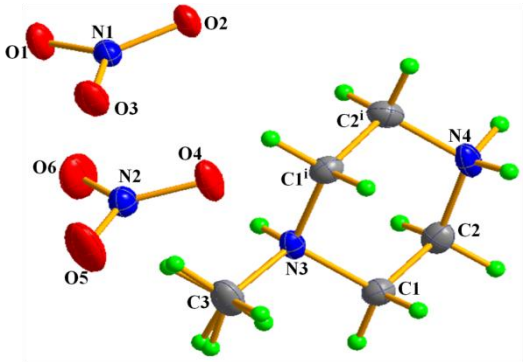
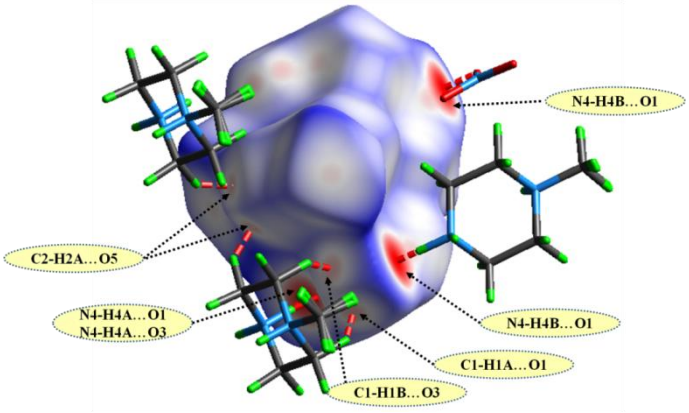
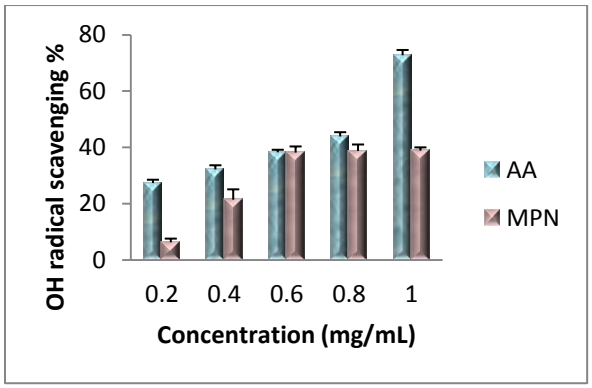

90
80
70
60
50
40
30
20
10
0
Reducing proprety %
0.2
0.4
0.6
0.8
1
Concentration (mg/mL)
AA
MPN

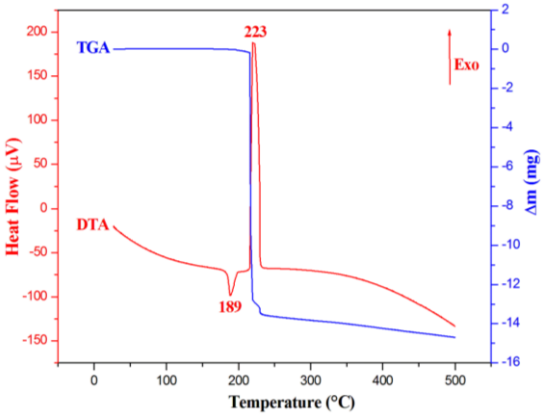
Fig. 14

Graphical Abstract









Tables captions

Table 1. Crystal data and experimental parameters used for the intensity data collection strategy and final results of the structure determination.

Table 2. Principal intermolecular distances (Å) and bond angles (°) in $[C_5H_{14}N_2](NO_3)_2$

Table 3. Hydrogen-bonds geometry (Å, °) in $[C_5H_{14}N_2](NO_3)_2$

Table 4. Enrichment ratio of different inter-contact and percentage of each atom on the surface Hirshfeld in $C_5H_{14}N_2(NO_3)_2$.

Table 1

Temperature	150K
Empirical formula	$[C_5H_{14}N_2](NO_3)_2$
Formula weight (g mol^{-1})	226.2
Crystal system	orthorhombic
Space group	*Pnma*
a	10.9385(9) Å
b	6.5698(4) Å
c	13.7021(10) Å
Z	4
V	984.68 (12) $Å^3$
F(000)	480
μ(Mo Kα)	0.14 mm^{-1}
Index ranges	$-8 \leq h \leq 8$, $-10 \leq k \leq 14$, $-17 \leq l \leq 13$
Reflections collected	3785
Independent reflections	1213
Reflections with $I > 2\sigma(I)$	961
R_{int}	0.046
Absorption correction: *multi-scan*	T_{min} = 0.883, T_{max} = 0.984
Refined parameters	92
$R[F^2 > 2\sigma(F^2)]$	0.044
$wR(F^2)$	0.101
Goodness of fit	1.07
$\Delta\rho_{max}$ = 0.234 e $Å^{-3}$	$\Delta\rho_{min}$ = -0.258 e $Å^{-3}$

Table 2

N1—O2	1.233 (2)	N3—C1	1.5005 (17)
N1—O3	1.261 (2)	C3—N3	1.485 (3)
N1—O1	1.263 (2)	C1—C2	1.507 (2)
N2—O5	1.232 (2)	N3—C1^{i}	1.5005 (17)
N2—O6	1.235 (2)	C2—N4	1.4905 (17)
N2—O4	1.258 (2)	N4—C2^{i}	1.4905 (18)
O2—N1—O3	120.80 (17)	N3—C1—C2	110.23 (12)
O2—N1—O1	120.49 (17)	N4—C2—C1	110.96 (12)
O3—N1—O1	118.70 (16)	C2—N4—C2^{i}	112.19 (16)
O5—N2—O6	121.65 (19)	C3—N3—C1^{i}	112.03 (10)
O5—N2—O4	118.62 (18)	C3—N3—C1	112.03 (10)
O6—N2—O4	119.73 (18)	C1^{i}—N3—C1	108.93 (15)

Symmetry code: (i) *x*, −*y*+3/2, *z*.

Table 3

D*—H···*A	***D*—H**	**H···*A***	***D*···*A***	***D*—H···*A***
N3—H3···O4	0.92 (3)	1.82 (3)	2.737 (2)	172 (3)
N3—H3···O5	0.92 (3)	2.58 (3)	3.282 (3)	133 (2)
N4—H4*A*···O3^{ii}	0.85 (3)	2.09 (3)	2.893 (2)	159 (3)
N4—H4*A*···O1^{ii}	0.85 (3)	2.38 (3)	3.103 (3)	143 (3)
N4—H4*B*···O1^{iii}	0.97 (3)	1.87 (3)	2.837 (2)	176 (2)
N4—H4*B*···O2^{iii}	0.97 (3)	2.49 (3)	3.077 (2)	119 (2)
C1—H1*A*···O1^{iv}	0.99	2.47	3.272 (2)	138
C1—H1*B*···O3^{v}	0.99	2.57	3.4753 (19)	153
C2—H2*A*···O5^{iv}	0.99	2.50	3.287 (2)	136

Symmetry code: (i i) −*x*−1/2, −*y*+1, *z*−1/2; (iii) −*x*, −*y*+1, −*z*+1; (iv) −*x*−1/2, *y*+1/2, *z*−1/2; (v) *x*, *y*+1, *z*.

Table 4

Enrichment	H	N	O
H	0.66	0.41	1.54
N			1.93
O			0.16
% Surface	59.1	1.45	39.2